Electronic Supplementary Material (ESI) for Materials Advances.

Supporting Information

High carrier mobility and ultralow thermal conductivity in the synthetic layered superlattice $Sn_4Bi_{10}Se_{19}$

Ruiming Lu,[1,⊥] Alan Olvera,[1,⊥] Trevor P. Bailey,[2] Jiefei Fu,[3] Xianli Su,[3] Igor Veremchuk,[4] Zhixiong Yin,[1] Brandon Buchanan,[1] Ctirad Uher,[2] Xinfeng Tang,[3] Yuri Grin,[4] Pierre F.P. Poudeu[1,]*

⊥ Contributed equally

**Corresponding Author*: Pierre Ferdinand Poudeu Poudeu

E-mail: ppoudeup@umich.edu; Fax: +1-734-763-4788

Content:

Details of materials synthesis and characterization methods;

Table S1: Selected crystallographic data for $Sn_4Bi_{10}Se_{19}$ at 300 K

Table S2: Wyckoff positions (W.P.), site occupancy factors (*k*), atomic coordinates, and equivalent isotropic displacement parameters ($U_{eq}/10^{-4}$ x Å^2) for all atoms in $Sn_4Bi_{10}Se_{19}$

Table S3: Selected inter-atomic distances (Å) in $Sn_4Bi_{10}Se_{19}$ at 300K

Table S4: Measured sound velocities and calculated elastic properties of $Sn_4Bi_{10}Se_{19}$ at 300K

Figure S1: Local environment of metal atoms in the structure of $Sn_4Bi_{10}Se_{19}$.

Figure S2: Rietveld refinement of phase fraction in S2 sample.

Figure S3: Differential Scanning Calorimetry (DSC) of $Sn_4Bi_{10}Se_{19}$ samples.

Figure S4: Schematic illustration of the "amorphous" structure of $Sn_4Bi_{10}Se_{19}$ (S1).

Figure S5: Temperature-dependent Hall Coefficient of the as-synthesized $Sn_4Bi_{10}Se_{19}$ sample (S1) and the sample after recrystallization (S2).

Synthesis of polycrystalline powder and crystal growth. To achieve single-phase polycrystalline powder samples of $Sn_4Bi_{10}Se_{19}$ with an excellent control over chemical composition, we adopted a multiple step synthesis approach involving a combination of solid-state reaction (SSR), induction melting and quenching (IMQ), and directional solidification (DS). In the first step, high purity elemental powder of Sn (+99.5%, Alfa Aesar), Bi (99% Alfa Aesar), and Se (99.5%, Sigma-Aldrich) were weighed in the stoichiometric ratio, thoroughly mixed using an agate mortar and pestle under Ar atmosphere in a glove box, and vacuum sealed in a quartz tube under a residual pressure of 10^{-5} Torr. Five sealed quartz tubes, each containing 3g of the elemental mixture were prepared in a similar manner. The tubes were loaded into a tube furnace, which was subsequently heated to 483 K in 6 h, and dwelled for 24 hours in order to allow low melting elements such as Se to react with Sn and Bi. The furnace was then heated to 823 K in 12 h, dwelled for 48 h and finally cooled to room temperature over 24 h. The products from the SSR step were dark-grey sintered ingots. In the second step, ingots obtained from the SSR step were melted and quenched multiple times (at least 5 times) using an induction furnace, without removing ingots from the original quartz tubes. The process ensures a homogeneous mixture of all the elements in the resulting high-density ingots, named samples S1. Melting and crystallization temperatures obtained from the differential scanning calorimetry (DSC) analysis of S1 samples, were then used to develop a heating profile for (1) the growth of single crystals suitable for X-ray structure determination, as well as (2) the fabrication of highly crystalline samples named S2, using the directional solidification process. Single crystals suitable for structure determination were obtained by annealing polycrystalline powder of sample S1 at 900 K for 120 hours. Highly crystalline samples were fabricated by heating high-density ingots obtained from the IMQ process (samples S1) at 973 K (just 50 ºC above the melting temperature) in 12 hours. After holding at this temperature for 1 hour, the furnace was allowed to slowly cool through the crystallization zone (from 973 K to 923 K) over 48 hours, followed by annealing at 923 K for another 48 hours, and finally rapid cooling to RT in 12 hours. The resulting samples (S2) were well-oriented, highly crystalline ingots. High-density pellets used for electronic and thermal transports measurements were obtained by consolidating polycrystalline fine powders of samples S1 and S2 at 723 K for 8 h using a uniaxial hot press under a residual pressure of 10^{-2} Torr and applied pressure of 100 MPa. The pellets were subsequently polished to mirror finish and used for thermal conductivity measurement. The pellets true density was measured using He gas pycnometry on a Quantachrome

Micro Ultrapyc 1200e pycnometer. For electronic transport measurements, prismatic bar specimens of dimensions $3 \times 2 \times 8$ mm^3 were cut from the hot pressed pellets using a wire saw.

Crystal structure determination. Several needle-shape dark-grey single crystals of $Sn_4Bi_{10}Se_{19}$ with approximate dimensions of $0.02 \times 0.04 \times 0.09$ mm^3 were selected from the sample mass and used for single-crystal X-ray diffraction study at 300 K. The crystals were mounted on the tips of glass fibers using two-component glue, and intensity data were collected using graphite-monochromated Mo_Kα radiation (λ = 0.71073 Å) on a STOE IPDS-2T diffractometer operated at 50 kV and 40 mA. The diffraction data was indexed in the monoclinic space group *C*2/*m* (#12) with lattice parameters a = 28.152(6) Å, b = 4.1567(8) Å, c = 21.242(4) Å, β =131(3)°, Z = 2 (Table S1). The structure solution was obtained using the direct methods, and the structure refinement was performed using least squares techniques in the SHELTXL package.[1-2] The structure solution revealed all seven heavy metal positions (Bi(1) to Bi(7)) and all ten selenium positions (Se(1) to Se(10)). The refinement of the initial model showed larger atomic displacement parameters for all the metal positions when compared to Se atoms. This suggests the intermixing of Bi with lighter atoms at these positions. Therefore, we considered mixed occupancy between Sn and Bi at all metal positions in the subsequent refinement cycles and assumed full occupancy of all sites. This model significantly improved the structure agreement parameters. The final refinement step, which included anisotropy parameters for all atoms and extinction correction, yielded the final structure refinement agreement factors. A summary of the crystallographic parameters for the structure refinement of $Sn_4Bi_{10}Se_{19}$ at 300 K is gathered in Table S1. The final distribution of Sn and Bi at all metal positions is reported in Table S2, along with the atomic coordinates and isotropic displacement parameters for all atoms in the crystal structure. Selected interatomic bond distances between metal atoms and selenium atoms forming the coordination environment are given in Table S3. The crystal structure of $Sn_4Bi_{10}Se_{19}$ (Figure 1) and the distorted coordination polyhedron formed by selenium atoms around various atoms (Figure S1) were created using the software Diamond.[3]

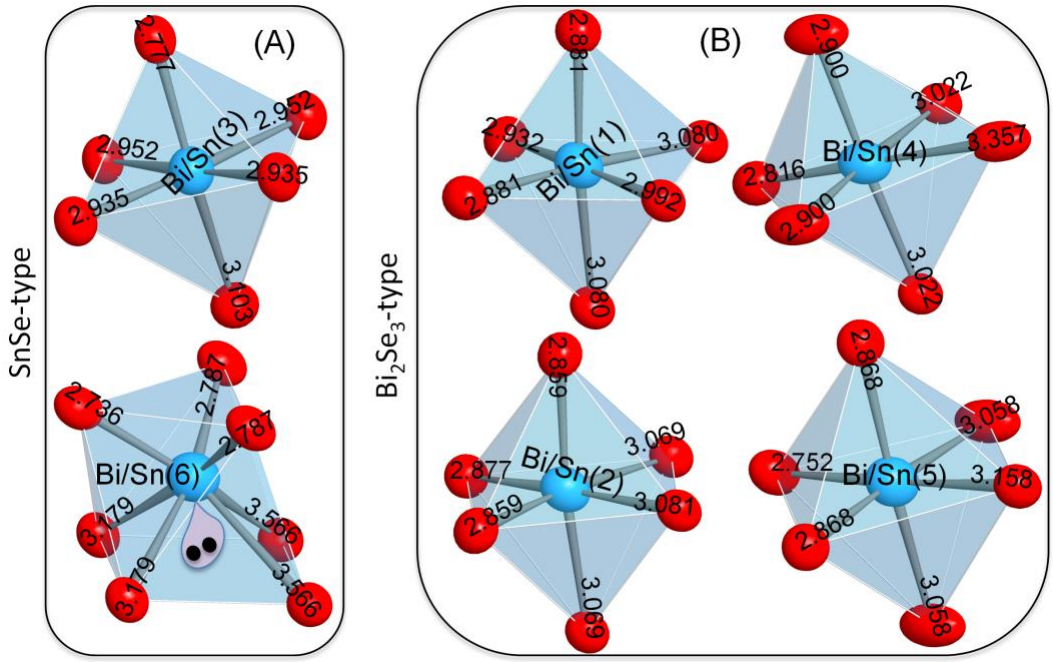

Figure S1: Local environment of metal atoms in the structure of $Sn_4Bi_{10}Se_{19}$. (A) Distorted coordination polyhedra formed by Se around metal atoms within the SnSe-type building block. (B) Distorted octahedra formed by Se around metal atoms within the Bi_2Se_3-type building block. Selenium atoms on the coordination polyhedron are labeled with the distance (in Å) from the central atom. M – Se contact much larger than the average bond distance of 3.05 Å is assumed to be a consequence of the repulsive forces from the lone electron pair.

Table S1. Selected crystallographic data for $Sn_4Bi_{10}Se_{19}$ at 300 K

Temperature	300 K
CCDC number	1942969
Formula Weight (g/mol)	4064.8
Crystal System; Space Group; Z	Monoclinic; *C*2/*m* (12); 2
Calc. Density (g/cm^3)	7.19
Cell Parameters	
a (Å)	28.152(6
b (Å)	4.1567(8)
c (Å)	21.242(4)
β (°)	130.97(3)
Cell Volume (Å^3)	1877(5)
Diffractometer; Radiation	IPDS-2T(Stoe); λ(MoK_α) = 0.71073 Å
μ (cm^{-1})	677
$2\theta_{max}$ (°); index range	58.4; -38 ≤ k ≤ 38, -5 ≤ h ≤ 5, -29 ≤ l ≤ 29
Residual elec. density [eÅ^{-3}]	+2.27 to -2.67
R_1 (F_o>4σ(F_o))[a]	0.026
wR_2 (all) [b]	0.066
GooF	1.08

[a] $R_1 = \Sigma||F_o|-|F_c||/\Sigma|F_o|$; [b] $wR_2 = [\Sigma w(F_o^2-F_c^2)^2/\Sigma w(F_o^2)^2]^{1/2}$

Table S2. Wyckoff positions (W.P.), site occupancy factors (*k*), atomic coordinates, and equivalent isotropic displacement parameters ($U_{eq}/10^{-4}$ x Å^2) in $Sn_4Bi_{10}Se_{19}$

Atom	*W.P*	*k*	*x*	*y*	*z*	U_{eq}
Bi1/Sn1	4i	0.84(2)/0.16(2)	0.1069(1)	1/2	0.0943(1)	215(1)
Bi2/Sn2	4i	0.74(2)/0.26(2)	0.0052(1)	0	0.1494(1)	208(1)
Bi3/Sn3	4i	0.80(2)/0.20(2)	0.2282(1)	1/2	0.4020(1)	200(1)
Bi4/Sn4	4i	0.52(2)/0.48(2)	0.2041(1)	0	0.0396(1)	213(1)
Bi5/Sn5	4i	0.80(2)/0.20(2)	0.0956(1)	1/2	-0.2049(1)	215(1)
Bi6/Sn6	4i	0.90(2)/0.10(2)	0.0985(1)	1/2	0.4569(1)	226(1)
Bi7/Sn7	4i	0.40(2)/0.60(2)	0.1558(1)	0	0.6787(1)	282(1)
Se1	2a	1.0	0	0	0	174(1)
Se2	4i	1.0	0.2006(1)	0	0.1691(1)	210(1)
Se3	4i	1.0	0.1010(1)	1/2	-0.0516(1)	178(1)
Se4	4i	1.0	0.2992(1)	1/2	0.1213(1)	263(1)
Se5	4i	1.0	0.0973(1)	1/2	0.2236(1)	207(1)
Se6	4i	1.0	0.1682(1)	0	0.4283(1)	166(1)
Se7	4i	1.0	0.2906(1)	0	0.3813(1)	180(1)
Se8	4i	1.0	0.0623(1)	0	0.5050(1)	188(1)
Se9	4i	1.0	-0.0029(1)	0	0.2776(1)	178(1)
Se10	4i	1.0	0.0777(1)	1/2	-0.3487(1)	191(1)

Table S3. Selected inter-atomic distances (Å) in $Sn_4Bi_{10}Se_{19}$ at 300K

Atoms 1,2	**d 1,2 [Å]**	**Atoms 1,2**	**d 1,2 [Å]**
Bi1|Sn1—Se2	2.881(2)	Bi5|Sn5—Se10	2.752(2)
Bi1|Sn1—Se2^{i}	2.881(2)	Bi5|Sn5—Se9^{iii}	2.868(1)
Bi1|Sn1—Se5	2.932(2)	Bi5|Sn5—Se9^{iv}	2.868(1)
Bi1|Sn1—Se3	2.992(2)	Bi5|Sn5—Se4^{vii}	3.058(2)
Bi1|Sn1—Se1	3.080(1)	Bi5|Sn5—Se4^{vi}	3.058(2)
Bi1|Sn1—Se1^{i}	3.080(1)	Bi5|Sn5—Se3	3.158(2)
Bi2|Sn2—Se5^{ii}	2.859(2)	Bi6|Sn6—Se7^{v}	2.736(2)
Bi2|Sn2—Se5	2.859(2)	Bi6|Sn6—Se8^{i}	2.787(1)
Bi2|Sn2—Se9	2.877(2)	Bi6|Sn6—Se8	2.787(1)
Bi2|Sn2—Se3^{iii}	3.069(2)	Bi6|Sn6—Se6	3.179(1)
Bi2|Sn2—Se3^{iv}	3.069(2)	Bi6|Sn6—Se6^{i}	3.179(1)
Bi2|Sn2—Se1	3.081(1)	**Bi6|Sn6—Se9^{i}**	**3.566(2)**
		Bi6|Sn6—Se9	**3.566(2)**
Bi3|Sn3—Se6^{v}	2.777(2)	**Bi6|Sn6—Se10^{iv}**	**3.865(2)**
Bi3|Sn3—Se7	2.935(1)		
Bi3|Sn3—Se7^{i}	2.935(1)	Sn7|Bi7—Se8	2.794(2)
Bi3|Sn3—Se6^{i}	2.952(1)	Sn7|Bi7—Se10^{viii}	2.795(1)
Bi3|Sn3—Se6	2.952(1)	Sn7|Bi7—Se10^{ix}	2.795(1)
Bi3|Sn3—Se5	3.104(2)	Sn7|Bi7—Se7^{v}	3.278(1)
		Sn7|Bi7—Se7^{x}	3.278(1)
Bi4|Sn4—Se2	2.816(2)	**Sn7|Bi7—Se4^{v}**	**3.550(2)**
Bi4|Sn4—Se4^{ii}	2.900(2)	**Sn7|Bi7—Se2^{v}**	**3.739(2)**
Bi4|Sn4—Se4	2.900(2)	**Sn7|Bi7—Se2^{x}**	**3.739(2)**
Bi4|Sn4—Se3	3.022(2)		
Bi4|Sn4—Se3^{ii}	3.022(2)		
Bi4|Sn4—Se4^{vi}	**3.357(2)**		

Operators for generating equivalent atoms:

(i) *x*, 1+*y*, *z*; (ii) *x*, –1+*y*, *z*; (iii) –*x*, –*y*, –*z*; (iv) –*x*, 1 –*y*, –*z*; (v) 1/2 –*x*, 1/2 –*y*, 1 –*z*; (vi) 1/2 –*x*, 1/2 –*y*, –*z*; (vii) 1/2 –*x*, 3/2 –*y*, –*z*; (viii) *x*, –1+*y*, 1+*z*; (ix) *x*, *y*, 1+*z*; (x) 1/2 –*x*, –1/2 –*y*, 1 –*z*; (xi) –*x*, –*y*, 1 –*z*; (xii) *x*, 1+*y*, –1+*z*; (xiii) *x*, *y*, –1+*z*.

Powder X-ray Diffraction. X-ray diffraction patterns of both the semi-crystalline (S1) and highly crystalline (S2) samples were collected using Cu-Kα radiation source on a Rigaku SmartLab diffractometer operating under the condition of 40 kV and 44 mA. The sample S1 obtained through SSR followed by IMQ process showed a completely different XRD pattern compared to the calculated pattern from single crystal data (Figure 2). However, the presence of clusters of high intensity diffraction peaks on the pattern suggests that the sample contains structural fragments with some degrees of short range ordering (partial crystallinity). Remarkably, after the directional solidification (DS) process, the XRD pattern of the resulting sample (S2) matched quite well the theoretical patterns calculated from single crystal data of $Sn_4Bi_{10}Se_{19}$ and $Sn_{4.11}Bi_{22.60}Se_{38}$, which are both members of the solid solutions series $Bi_{2x}Sn_{38-3x}Se_{38}$, indicating improved ordering of the atomic structure (Figure 2). However, the refinement of phase composition indicates the presence of both $Sn_4Bi_{10}Se_{19}$ and $Sn_{4.11}Bi_{22.60}Se_{38}$ phases along with a small fraction of metallic Bi (Figure S2). Despite the sharp difference between the XRD patterns of samples S1 and S2, we speculate that sample S1 contains some structural and chemical features also present in sample S2, which facilitate full crystallization during the directional solidification step. The above analysis is further confirmed by differential scanning calorimetry (DSC) studies.

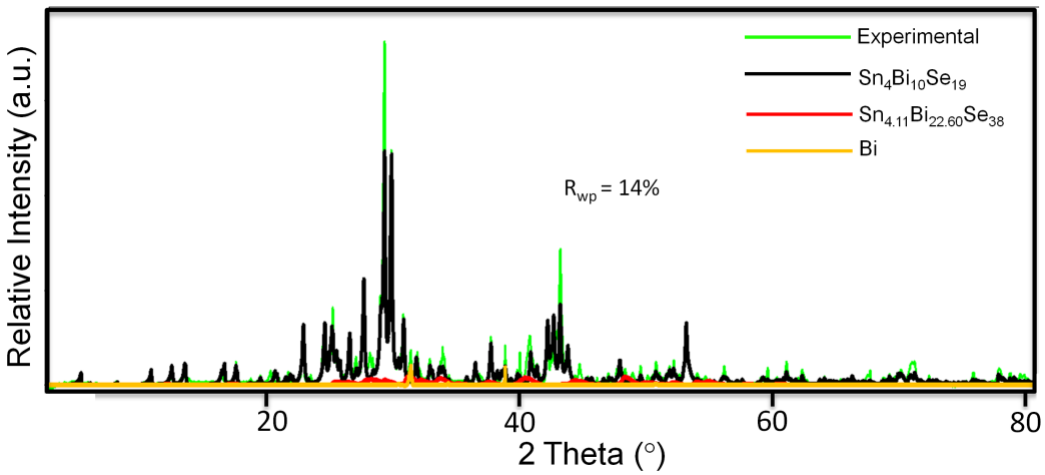

Figure S2: Rietveld refinement of phase fraction in S2 sample. Black: $Sn_4Bi_{10}Se_{19}$; Red: $Sn_{4.11}Bi_{22.60}Se_{38}$; and Orange: metallic Bi impurity.

Differential Scanning Calorimetry (DSC). Melting and crystallization temperatures of the synthesized samples (S1 and S2) were obtained using differential scanning calorimetry (DSC) data collected on a Netzsch DSC404F1 system. Approximately 30 mg of finely ground polycrystalline powder were sealed inside small quartz capillary tubes under a residual pressure of 10^{-5} Torr. An empty quartz capillary tube sealed under similar condition was used as the reference during the measurement. The measurements were performed from room temperature to 1273 K in two heating-and-cooling cycles under an atmosphere of flowing nitrogen gas in order to evaluate the thermal stability of the compound upon melting.

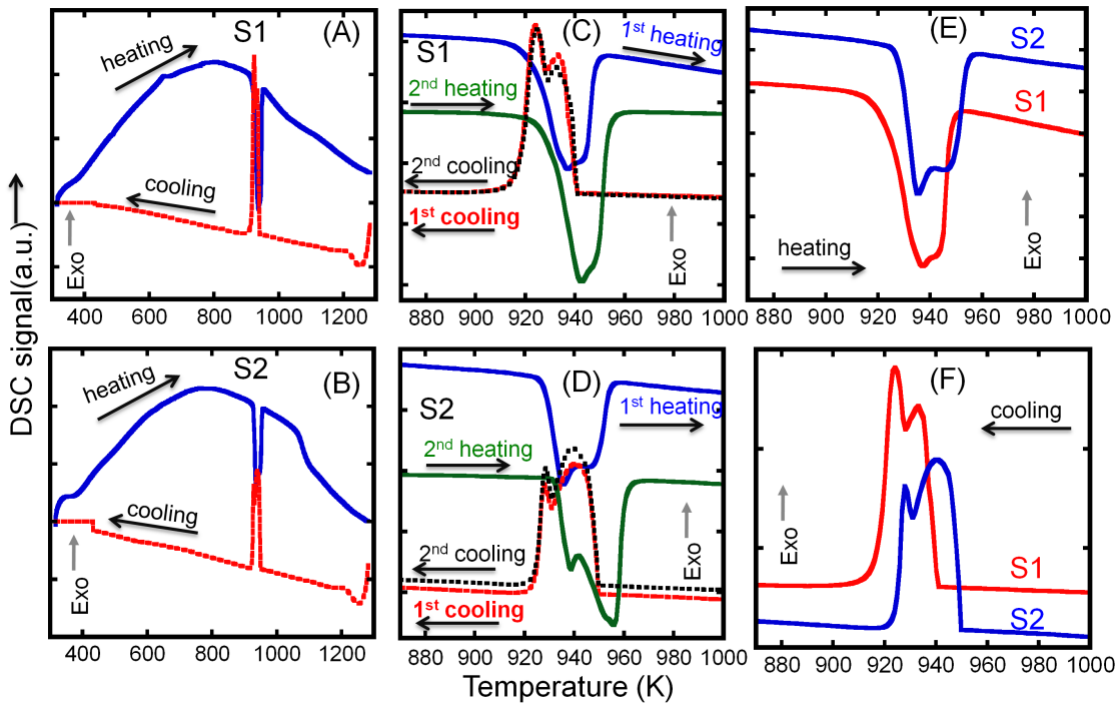

Figure S3: Differential Scanning Calorimetry (DSC) of $Sn_4Bi_{10}Se_{19}$ samples. (A) Heating and cooling curves of the as-synthesized sample (S1); (B) heating and cooling curves of the sample obtained after recrystallization (S2); two heating and cooling cycles for samples S1 (C) and S2 (D) highlighting the thermal stability of the samples upon melting; Comparison of the first heating curves (E) and the first cooling curves (F) for samples S1 and S2 showing a small increase in the melting and crystallization temperatures after the recrystallization process.

The S1 and S2 samples showed very similar DSC heating and cooling curves (Figure S3A and S3B). Both samples exhibit a broad melting endothermic event with peak around 940 K on the first heating curves (Figure S3E, S3F). The exothermic crystallization event is also broad with a peak around 940 K. Additional thermal event that would suggest the presence of impurity phases could not be observed on the DSC curves. Even the melting peak that would be anticipated at 544 K for the metallic Bi impurity observed on the XRD data of S2 sample is also missing, suggesting its significantly small fraction. The only major difference in the first DSC heating curves of samples S1 and S2 is the presence of two peaks at 940 K and 943 K on the heating curve of sample S2, which is not well resolved in sample S1. Also, the onset temperature of the melting and crystallization peaks for the sample S2 is slightly shifted to higher temperature. The above analysis further supports some degrees of similarities in the atomic structure and chemical bonding between the S1 and S2 samples. Therefore, we proposed that the S1 sample is a relatively disordered "amorphous" phase of $Sn_4Bi_{10}Se_{19}$, which contains several structural fragments found in the highly

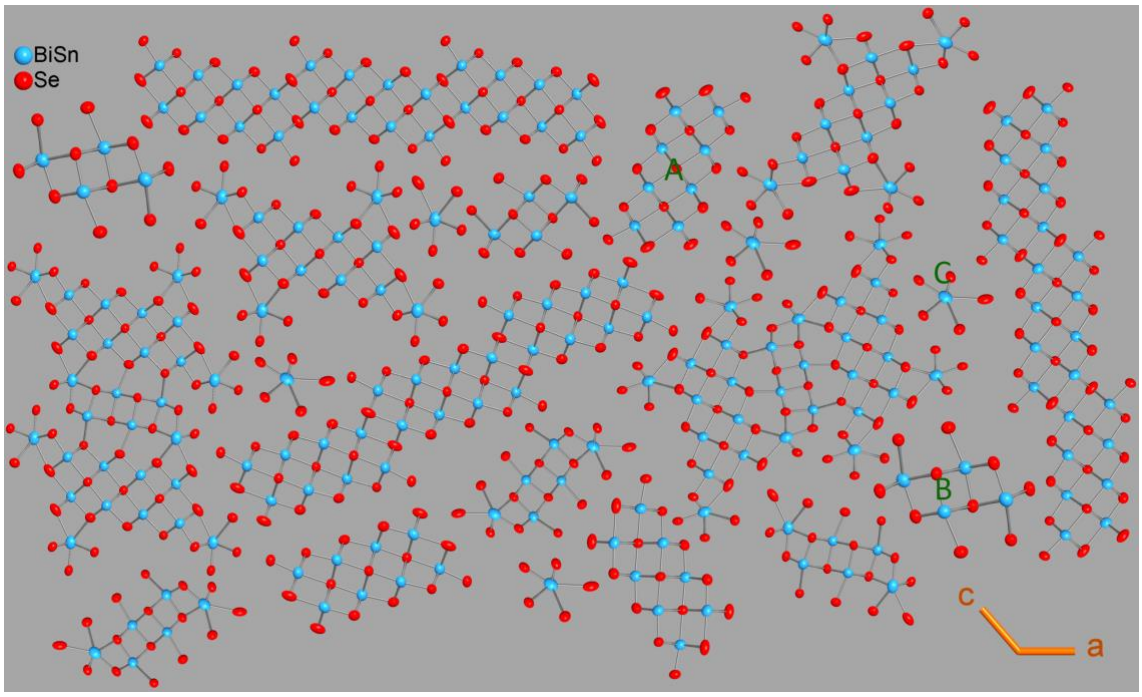

Figure S4: Schematic illustration of the poorly crystallized structure of the S1 sample of $Sn_4Bi_{10}Se_{19}$. Various structural fragments formed by the building blocks A, B, and C are randomly assembled into a semi-crystalline structure that features short-range atomic order within the fragments and lack of long-range periodicity.

crystalline sample S2 but lacks long range ordering (Figure S4). The $Sn_4Bi_{10}Se_{19}$ phase melts and crystallizes with a remarkable thermal stability **(**Figure S3C, S3D).

Electronic transport and thermal property measurements. Electrical conductivity and Seebeck coefficient were measured simultaneously on a bar-shape specimen of $Sn_4Bi_{10}Se_{19}$ samples (S1 and S2) using the four-probe method on a commercial ULVAC-RIKO ZEM-3 system. The data were recorded from room temperature to 775 K under a low-pressure helium atmosphere using rectangular bars of dimensions $3 \times 2 \times 8$ mm^3. The instrument precision for electrical resistivity and thermopower data is ± 4%.

The specific heat capacity and thermal diffusivity were measured on a laser flash system (Linseis LFA-1000) from room temperature to 775 K. The surface of the hot-pressed pellets from samples S1 and S2 were cleaned and lightly coated with thin graphite film prior to measurement. Thermal diffusivity and specific heat data were measured from 300 to 775 K under flowing N_2 gas (>30 mL/min). The accuracy of the data was determined to be within 2% of the equipment precision of ±4%. The thermal conductivity was calculated using the equation $\kappa_{tot} = \rho C_P D$, where ρ, C_P and D are, respectively, the density, specific heat capacity and thermal diffusivity of the samples.

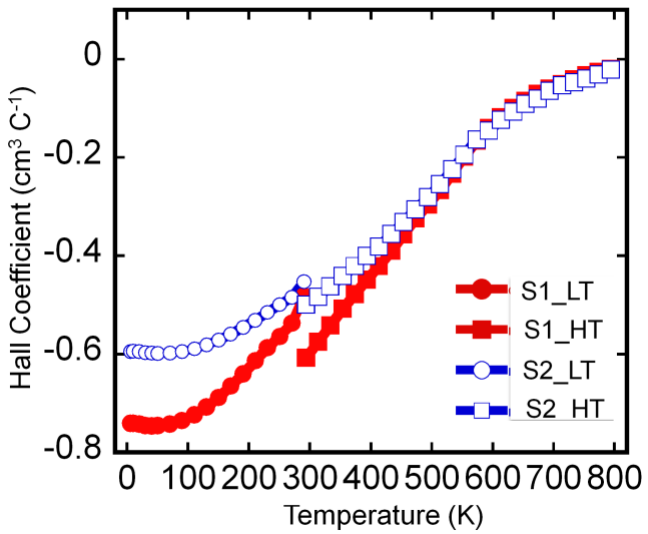

Figure S5: Temperature-dependent Hall Coefficient of the as-synthesized $Sn_4Bi_{10}Se_{19}$ sample (S1) and the sample after recrystallization (S2).

The density of the pressed pellets was measured using He gas pycnometry on Micromeritics Accupyc II 1340.

To evaluate the carrier concentration and carrier mobility of the samples, low-temperature and high-temperature Hall effect measurements (Figure S5) were performed under a magnetic field of 1 T using a home-built apparatus.

Heat Capacity. Low temperature heat capacity (C_p) data was measured on the highly crystalline sample (S2) from 2 K to 400 K using a PPMS system. A small dab of N-grease was placed on the sample holder for the addendum measurement without the sample, and then a polished thin piece of the S2 ingot weighing approximately 20 mg was placed flat on the greased stage for the sample measurement. The final C_p data (Figure 3D) was obtained by subtracting the addendum measurement from the sample measurement.

The initial heat capacity rapidly increases with temperatures and then plateaus at 0.19 J g^{-1} K^{-1} between 300 K and 400 K, which is similar to the Dulong-Petit value (0.20 J g^{-1} K^{-1}). The heat capacity under 10 K was fitted with the Debye model ($C_p = \varphi T + \beta T^3 + \alpha T^5$) and plotted as C_p/T vs. T^2 (inset of Figure 3D). The fitted β value of 0.0212 J mol^{-1} K^{-2} was used to calculate the Debye temperature (Θ_D = 182 K) according to the equation
$\Theta^3 = (12\pi 4R)/(5\beta)$, where R is the molar gas constant.

Sound velocities and elastic properties. The elastic properties such as shear modulus *G*, Poison's Ratio υ, bulk modulus *B*, Young's modulus *E* and average sound velocity υ_m, as well as the Debye temperature, θ, and Grüneisen parameter γ, (Table S4) were calculated from sound velocity measurements using the following equations:

$$G = \rho \cdot v_s^2 \quad (1)$$

$$E = \frac{[\rho v_s^2 (v_l^2 - 4v_s^2)]}{(v_l^2 - v_s^2)} \quad (2)$$

$$\nu = \frac{[1 - 2(\frac{v_s}{v_l})^2]}{2[1 - (\frac{v_s}{v_l})^2]} \quad (3)$$

$$B = \frac{2}{3}\left(\frac{1+\nu}{1-2\nu}\right) G \quad (4)$$

$$v_m = [\frac{1}{3}(\frac{2}{v_s^3} + \frac{1}{v_l^3})]^{-1/3} \quad (5)$$

$$\theta = \frac{h}{k}\left(\frac{3q}{4\pi}\frac{N\rho}{M}\right)^{1/3}\upsilon_m \quad (6)$$

$$\gamma = \frac{3}{2}\left(\left(\frac{1+\nu}{2-3\nu}\right)\right) \quad (7)$$

where ρ is the measured density of the bulk sample (7.19 g cm^{-3} for our measured $Sn_4Bi_{10}Se_{19}$), h the Planck constant, k the Boltzmann constant, N the Avogadro number, q the number of atoms per chemical formula and M the molar mass per formula.[4-6]

Sound velocity data was obtained by the ultrasonic pulse-echo method. Longitudinal/ transverse ultrasonic waves produced by an ultrasonic transducer (which is also used as the sound detector), attached to the surface of the sample travel across the thickness direction and bounce between the top and bottom surfaces, giving an echoing signal. With the echoing period Δt and the thickness of sample, d, the longitudinal sound velocity, υ_l, and transverse sound velocity, υ_s, were extracted and used for the calculation of the elastic properties.

Table S4. Measured sound velocities and calculated elastic properties of $Sn_4Bi_{10}Se_{19}$ at 300K

List of Properties	Values
Longitudinal Sound Velocity, υ_l	2870.8 m/s
Transverse Sound Velocity, υ_s	1673.8 m/s
Average Sound Velocity, υ_m	1856.6 m/s
Poisson's Ratio, υ	0.243
Shear Modulus, G	20.68 GPa
Bulk Modulus, B	51.40 GPa
Young's Modulus, E	33 GPa
Debye Temperature, θ	182 K
Gruneisen Parameter, γ	1.86

Calculation of lattice thermal conductivity (κ_{L0}). The theoretical "intrinsic" lattice thermal conductivity (κ_{L0}), within the temperature range where only acoustic phonons conduct heat was calculated using the equation (S1).

$$\kappa_{L0} = A\,[(M\Theta^3\delta)/(\gamma^2 n^{2/3}\mathrm{T})] \quad (S1)\ [7]$$

where M is the average mass of the atoms within the crystal; Θ is the Debye temperature; n is the number of atoms in the primitive unit cell of the crystal; δ is the volume per atom; γ is the high temperature limit of the acoustic phonon mode Grüneisen parameter; A is a constant taken as 3.1 x 10^{-6} if κ is given in W m^{-1} K^{-1}; M is in atomic mass units (amu or gram per mole) and δ is in Å.

For $Sn_4Bi_{10}Se_{19}$, n = 66, M = 123.2 amu, and δ = 3.05 Å. The materials parameters γ and Θ were obtained from the elastic properties using the equations (S2) and (S3), respectively. [4-6]

$$\gamma = \frac{3}{2}\left(\frac{1+\nu}{2-3\nu}\right) \qquad \text{(S2)}$$

and

$$\theta = \frac{h}{k}\left(\frac{3q}{4\pi}\frac{N\rho}{M}\right)^{1/3} \upsilon_m \qquad \text{(S3)}$$

where ρ is the measured density of the bulk $Sn_4Bi_{10}Se_{19}$ sample (ρ = 7.19 g cm^{-3}), h the Planck constant, k the Boltzmann constant, N Avogadro's number, and q the atom number per chemical formula. Elastic properties calculated from sound velocity measurement are summarized in Table S4.

Reference

(1) Sheldrick, G. *SHELXTL, DOS Windows/NT*, version 6.12; Bruker analytical X-ray instruments Inc.: Madison, WI, USA, 2000.

(2) Sheldrick, G. M., Crystal structure refinement with SHELXL. *Acta Crystallogr C* **2015,** *71* (1), 3-8.

(3) Brandenburg, K.; Putz, H. *DIAMOND*, Version 3.0 c; Crystal Impact GbR: Bonn, Germany, 2005.

(4) Sanditov, D. S.; Belomestnykh, V. N., Relation between the parameters of the elasticity theory and averagedbulk modulus of solids. *Tech Phys* **2011,** *56* (11), 1619-1623.

(5) Sanditov, D. S.; Mantatov, V. V.; Darmaev, M. V.; Sanditov, B. D., On the Gruneisen parameter for crystals and glasses. *Tech Phys* **2009,** *54* (3), 385-388.

(6) Anderson, O. L., A simplified method for calculating Debye temperature from elastic constants. *J Phys Chem Solids* **1963,** *24* (7), 909-917.

(7) Morelli, D. T.; Jovovic, V.; Heremans, J. P., Intrinsically minimal thermal conductivity in cubic I-V-VI_2 semiconductors. *Phys Rev Lett* **2008,** *101* (3), 035901.